J|A|C|S
ARTICLES
Published on Web 02/19/2004

Reaction Intermediates in Acid Catalysis by Zeolites: Prediction of the Relative Tendency To Form Alkoxides or Carbocations as a Function of Hydrocarbon Nature and Active Site Structure

M. Boronat,[†] P. M. Viruela,[‡] and A. Corma*,[†]

Contribution from the Instituto de Tecnología Química, UPV-CSIC, Universidad Politécnica de Valencia, Avd/dels Tarongers, s/n, 46022 Valencia, Spain, and Departament de Química Física, Universitat de Valencia, C/Dr. Moliner 50, 46100 Burjassot, Spain

Received November 5, 2003; E-mail: acorma@itq.upv.es

Abstract: The mechanism of protonation of ethene, propene, and isobutylene adsorbed on seven different Brønsted acid sites of mordenite has been studied at the ONIOM (B3PW91/6-31G(d,p):MNDO) theoretical level to assess the influence of olefin size and local geometry of the active site on the species and energies involved. The activation energies for olefin protonation are determined by short- and medium-range electrostatic effects and reflect the order of stability of primary, secondary, and tertiary carbenium ions. On the other hand, the stability of covalent alkoxides depends linearly on the AlO_bSi angle value in the complex, which in turn is determined by the corresponding value in the deprotonated zeolite. It is also shown that the mechanism of protonation of isobutylene is different from that of ethene and propene and involves a free *tert*-butyl carbenium ion as a true reaction intermediate. Whether this carbenium ion is converted into a covalent alkoxide depends on the T position on which the Al is located. All these findings allow us to predict, on the basis of the position and local geometry of the Brønsted acid site, whether the reaction intermediates of olefin protonation will be covalent alkoxides or free carbenium ions.

1. Introduction

Acid zeolites are widely used in petroleum and chemical industries as solid catalysts for a number of commercially important hydrocarbon reactions. Besides their high activity, selectivity, and thermal stability, their microporous structure provides a large internal surface and important selectivity effects related both to diffusion of reactants and products inside the pore system and to steric constraints on reaction intermediates and transition states.[1] It has been frequently assumed that reaction mechanisms on acid zeolites are analogous to those in the gas phase or in superacid media and that free carbenium and carbonium ions are the intermediate species formed by interaction of hydrocarbon molecules with the zeolite Brønsted acid sites.[2−4] The development of experimental techniques for the in situ study of reactions on solids, such as variable temperature solid-state NMR[5,6] and FT-IR,[7] has made possible the direct observation of the Brønsted acid sites and their interaction with adsorbed molecules. It has been shown that simple carbenium ions are not stable species within the zeolite channels, and only some cyclic cations, in which the positive charge is delocalized and sterically inaccessible to framework oxygens, have been experimentally observed on the surface of acidic zeolites.[5] Instead, alkoxide species with the alkyl group covalently bonded to the framework oxygens have been found to be important long-lived intermediates in the reactions of propene on zeolites HY,[8] H-ZSM-5,[9] and H-mordenite[9] or in the adsorption of 2-methyl-2-propanol on H-ZSM-5.[10] In other cases, as for example adsorption and reactions of isobutylene on HY,[11] H-ZSM-5,[11] or H-mordenite,[12] neither the *tert*-butyl carbenium ion nor the *tert*-butoxide covalent species has been experimentally observed, and therefore, the nature of the reaction intermediates in this case is not clear yet.

The interaction of small olefins with zeolite Brønsted acid sites has been the subject of several quantum chemical studies,[13−20] and the results obtained are dependent on the

[†] Universidad Politécnica de Valencia.
[‡] Universitat de Valencia.

(1) Corma, A. *J. Catal.* **2003**, *216*, 298−312.
(2) Olah, G. A.; Prakash, G. K. S.; Sommer, J. *Superacids*; Wiley-Interscience: New York, 1995.
(3) Olah, G. A.; Prakash, G. K. S.; Williams, R. E.; Field, J. D.; Wade, D. *Hydrocarbon Chemistry*; Wiley & Sons: New York, 1987.
(4) Jacobs, P. A. *Carboniogenic Activitiy of Zeolites*; Elsevier: New York, 1977.
(5) Haw, J. F. *Phys. Chem. Chem. Phys.* **2002**, *4*, 5431−5441, and references therein.
(6) Haw, J. F.; Nicholas, J. B.; Xu, T.; Beck, L. W.; Ferguson, D. B. *Acc. Chem. Res.* **1996**, *29*, 259−267.
(7) Farneth, W. E.; Gorte, R. J. *Chem. Rev.* **1995**, *95*, 615−635.
(8) Haw, J. F.; Richardson, B. R.; Oshiro, I. S.; Lazo, N. D.; Speed, J. A. *J. Am. Chem. Soc.* **1989**, *111*, 2052−2058.
(9) Geobaldo, F.; Spoto, G.; Bordiga, S.; Lamberti, C.; Zecchina, A. *J. Chem. Soc., Faraday Trans.* **1997**, *26*, 1243−1249.
(10) Aronson, M. T.; Gorte, R. J.; Farneth, W. E.; White, D. *J. Am. Chem. Soc.* **1989**, *111*, 840−846.
(11) Lazo, N. D.; Richardson, B. R.; Schettler, P. D.; White, J. L.; Munson, E. J.; Haw, J. F. *J. Phys. Chem.* **1991**, *95*, 9420−9425.
(12) Ishikawa, H.; Yoda, E.; Kondo, J. N.; Wakabayashi, F.; Domen, K. *J. Phys. Chem. B* **1999**, *103*, 5681−5686.
(13) Kazansky, V. B. *Acc. Chem. Res.* **1991**, *24*, 379−383.
(14) Viruela, P.; Zicovich-Wilson, C. M.; Corma, A. *J. Phys. Chem.* **1993**, *97*, 13713−13719.

10.1021/ja039432a CCC: $27.50

Chart 1. Structures of Olefin Adsorbed on a Brønsted Acid Site (I), Transition State for the Olefin Protonation Reaction II, Alkoxide Complex (III), and Adsorbed Carbenium Ion (IV)

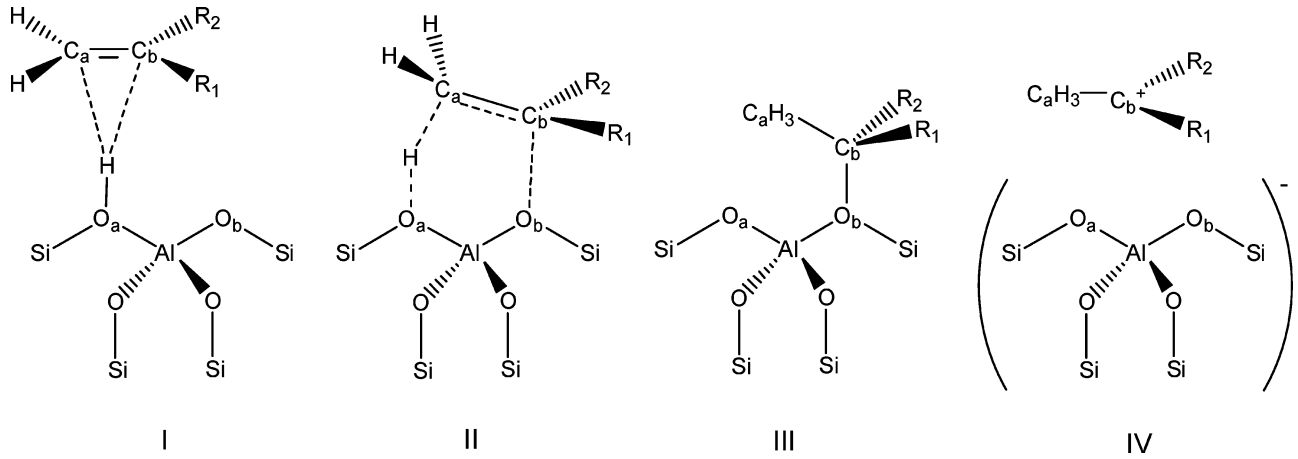

I II III IV

theoretical method and the model size used to simulate the solid catalyst. In the pioneering work of Kazansky et al.[13] it was proposed that protonation of an olefin by an acid hydroxyl group results in formation of a more stable covalent alkoxide species. According to this mechanism, depicted in Chart 1, the process is concerted and occurs through a transition state in which the geometry and electronic structure of the organic fragment resembles that of a classical carbenium ion. In this and other studies,[14,15] the solid was simulated by means of a small cluster of atoms (typically $HO(H)-Al(OH)_3$, $SiX_3-OH-AlX_3$, or $SiX_3-OH-AlX_2-OSiX_3$). The cluster approach is well-suited to describe local phenomena such as the interactions of molecules with active sites or bond breaking and bond formation processes because it allows for the use of high quality theoretical methods. However, this methodology shows important limitations because it neglects the long-range electrostatic effects caused by the Madelung potential of the crystal, and since the models used are not typical of any particular zeolite, they are not able to explain the different catalytic behavior exhibited by structurally different zeolites. To address this situation, some studies of ethene, propene, and isobutylene protonation by different zeolites have appeared in the literature that use larger clusters,[16,17] combined quantum mechanics/molecular mechanics (QM/MM) methods,[18] or periodic calculations.[17,19,20] In all cases, it was found that the stability of the alkoxide complexes is very sensitive to the local geometry of the active sites, with the *tert*-butoxide complexes being the most affected by this factor. A recent periodic DFT study of isobutylene adsorption in three acid zeolites (CHA, TON, and MOR)[20] concluded that steric constraints due to the crystalline structure of a particular zeolite are important enough to make, in some cases, the covalent *tert*-butoxide species as unstable as the *tert*-butyl carbenium ion. Thus, the role of carbenium ions in zeolite-catalyzed hydrocarbon reactions is still a question of debate.

In this work, the mechanism of protonation of ethene, propene, and isobutylene by seven different Brønsted acid sites in H-mordenite has been studied using the ONIOM methodology. Our main objective was to analyze the influence of both the olefin size and the local geometry of the active site in a particular position of a given zeolite on the energies involved in the mechanism of olefin protonation by Brønsted acid sites. In agreement with previous work,[17b,18,19] it has been found that the stability of the covalent alkoxides is marked by the olefin size and follows the order ethoxide > propoxide > *tert*-butoxide, while the activation energies for protonation are mainly influenced by medium-range electrostatic effects and reflect the order of stability of primary, secondary, and tertiary carbenium ions. The most interesting results obtained in this work are those related with the influence of the position of the active site on the reaction mechanism. First, it has been found that the stability of a given alkoxide depends linearly on the AlO_bSi angle value in the deprotonated zeolite, making it possible to predict which positions in a given zeolite are favorable for formation of stable alkoxide intermediates. Second, it is shown that the mechanism of protonation of isobutylene is different from that of ethene and propene and involves a free *tert*-butyl carbenium ion as a true reaction intermediate.

2. Models and Methods

Figure 1 shows the projection of the mordenite lattice along the *c* and *b* axes, with the atom-labeling scheme. The silicon framework of mordenite is composed of four- and five-membered rings which link to form large 12-T ring channels parallel to *c* interconnected via 8-T ring side pockets parallel to *b*. There are four inequivalent tetrahedral sites in the mordenite unit cell. T1 is in the 12-T ring main channel, T2 and T4 are in the intersection between the 12-T channel and the 8-T pocket, and T3 is inside the 8-T pocket. Mordenite crystallizes in an orthorhombic *Cmcm* space group with lattice parameters $a = 18.094$, $b = 20.516$, and $c = 7.524$[21] Å and has 144 atoms in the conventional unit cell.

In the first step, the structure of pure-silica mordenite was optimized with molecular mechanics (MM) techniques using the GULP code[22] and the shell-model force field derived by Schröder and Sauer.[23] Taking this structure as the starting point, an Al atom was introduced into every one of the four inequivalent positions, and the geometries of the

(15) Boronat, M.; Viruela, P.; Corma, A. *J. Phys. Chem. A* **1998**, *102*, 982−989.
(16) Mota, C. J. A.; Esteves, P. M.; de Amorim, M. B. *J. Phys. Chem.* **1996**, *100*, 12418−12423.
(17) (a) Boronat, M.; Zicovich-Wilson, C. M.; Viruela, P.; Corma, A. *Chem.−Eur. J.* **2001**, *7*, 1295−1303. (b) Boronat, M.; Zicovich-Wilson, C. M.; Viruela, P.; Corma, A. *J. Phys. Chem. B* **2001**, *105*, 11169−11177.
(18) Sinclair, P. E.; de Vries, A.; Sherwood, P.; Catlow, C. R. A.; Van Santen, R. A. *J. Chem. Soc., Faraday Trans.* **1998**, *94*, 3401−3408.
(19) Rozanska, X.; Demuth, Th.; Hutschka, F.; Hafner, J.; Van Santen, R. A. *J. Phys. Chem. B* **2002**, *106*, 3248−3254.
(20) Rozanska, X.; Van Santen, R. A.; Demuth, Th.; Hutschka, F.; Hafner, J. *J. Phys. Chem. B* **2003**, *107*, 1309−1315.
(21) Alberti, A.; Davoli, P.; Vezzalini, G. *Z. Krystallogr.* **1986**, *175*, 249−256.
(22) Gale, J. D. The General Utility Lattice Program (GULP); Royal Institution/Imperial College: London, 1992−1994.
(23) Schröder, K. P.; Sauer, J. *J. Phys. Chem.* **1996**, *100*, 11043−11049.

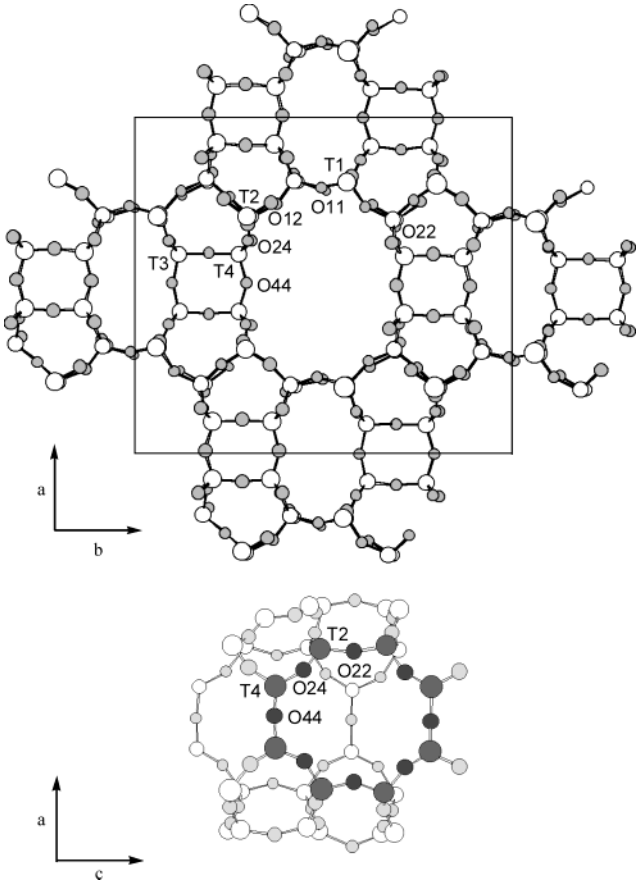

Figure 1. Structure of mordenite framework showing the atom labeling scheme.

Table 1. Relative and Deprotonation Energies (kcal/mol), OH Bond Lengths (angstroms), and Vibrational Frequencies[a] (cm^{-1}) of the Mordenite Brønsted Acid Sites Considered in This Work

name	Al–O_a	O_b	E_{rel} (MM)[b]	DPE (MM)	DPE (QM)	r(OH) (QM)	ν(OH) (QM)
T1A	T1−O11	O12	1.54	260.9	303.2	0.970	3651.7
T1B	T1−O12	O11	0.96	261.4	302.9	0.973	3607.0
T2A	T2−O12	O24	1.28	260.6	298.7	0.972	3615.1
T2B	T2−O22	O24	1.07	260.8	303.0	0.974	3584.2
T2C	T2−O24	O12, O22	1.49	260.4	304.1	0.968	3666.4
T4A	T4−O24	O44	0.00	261.1	297.6	0.971	3637.2
T4B	T4−O44	O24	7.64	253.8	294.5	0.973	3593.5

[a] Scaled by 0.9573.[32] [b] The labeling of the O atoms is shown in Figure 1.

resulting deprotonated systems were optimized. The order of stability of the different positions was T4 < T3 < T2 < T1, but T1 was only 1.26 kcal/mol less stable than T4. Then, Brønsted acid sites were created by introducing one H atom into the structures obtained for the Al in T1, T2, and T4 positions. The proton was placed only on those O atoms linked to Al that resulted in a bridging hydroxyl group pointing toward either the 12-T main channel or to the intersection between the 12-T channel and the 8-T pocket. By excluding T3 and the H atoms pointing toward the 5-T or 8-T inner rings, we made sure that all the active sites studied were accessible to organic molecules. The name, atom labeling, and relative stability of the acid sites considered in this work are summarized in Table 1.

Three clusters of atoms were then cut out from the structures obtained for the deprotonated systems with the Al atom in the T1, T2, and T4 positions. They contained the Al atom, four coordination spheres around this, one complete 12-T ring, and one complete 8-T pocket. The dangling bonds that connected the cluster to the rest of the solid were saturated with H atoms at 1.49 Å from the Si atoms and orientated toward the positions occupied in the crystal by the oxygen atoms in the next coordination sphere. The size of the clusters modeling T1, T2, and T4 was 148, 125, and 130 atoms, respectively. Using these clusters to simulate the solid catalyst, we optimized the geometries of the seven Brønsted acid sites summarized in Table 1, the adsorbed olefins, the transition states for the olefin protonation reaction, and the alkoxide and/or carbenium ion products by means of the ONIOM scheme[24] as implemented in the Gaussian 98 computer program.[25]

The ONIOM approach subdivides the *real* system into several parts or layers, each of which is described at a different level of theory. The most important one is called the *model* system and is described at the highest level of theory, while subsequent layers are computed at progressively lower and computationally cheaper levels of theory. In the ONIOM approach, the total energy of a system subdivided into two layers is aproximated as:

$$E^{\mathrm{ONIOM}} = E\,(\mathrm{high, model}) + E\,(\mathrm{low, real}) - E\,(\mathrm{low, model})$$

In the present work, the model system included the Al atom, the four O atoms in the first coordination sphere, the four Si atoms bonded to them, the proton of the Brønsted acid site, and the organic molecules studied. The coordinates of these atoms were completely optimized using the density functional B3PW91[26] method and the standard 6-31G-(d,p) basis set.[27] The rest of the system was treated at the semiempirical MNDO level,[28] and no geometry optimization was performed. The nature of every stationary point was characterized by means of frequency calculations and analysis of the vibrational modes. Since these systems were constrained stationary points due to the restrictions imposed on the low level layer of the real system, some imaginary vibrational modes with frequencies lower than 100 cm^{-1} were sometimes obtained. It was checked in all cases that they were related to the movement of the framework atoms whose position was not optimized in the calculations, and not to the atoms involved in the reaction path. The calculated energies of all structures were corrected for the zero-point vibrational energies (ZPE) obtained from the frequency calculations.

3. Results and Discussion

3.1. Active Sites. Table 1 summarizes the relative stability of the seven mordenite Brønsted acid sites considered in this work at the MM level, the deprotonation energies calculated at both MM and QM levels, and the OH bond lengths and vibrational frequencies obtained at the QM level. At the MM level, the stability of all sites except T4B is similar. At the QM level, it is not possible to directly compare the energies of all sites because of the different stoichiometry of the three clusters used. However, deprotonation energies calculated as the energy difference between the Brønsted acid site and the deprotonated

(24) (a) Svensson, M.; Humbel, S.; Froese, R. D. J.; Matsubara, T.; Sieber, S.; Morokuma, K. *J. Phys. Chem.* **1996**, *100*, 19357−19363. (b) Humbel, S.; Sieber, S.; Morokuma, K. *J. Chem. Phys.* **1996**, *105*, 1959−1967.
(25) Frisch, M. J.; Trucks, G. W.; Schlegel, H. B.; Scuseria, G. E.; Robb, M. A.; Cheeseman, J. R.; Zakrzewski, V. G.; Montgomery, J. A., Jr.; Stratmann, R. E.; Burant, J. C.; Dapprich, S.; Millam, J. M.; Daniels, A. D.; Kudin, K. N.; Strain, M. C.; Farkas, O.; Tomasi, J.; Barone, V.; Cossi, M.; Cammi, R.; Mennucci, B.; Pomelli, C.; Adamo, C.; Clifford, S.; Ochterski, J.; Petersson, G. A.; Ayala, P. Y.; Cui, Q.; Morokuma, K.; Malick, D. K.; Rabuck, A. D.; Raghavachari, K.; Foresman, J. B.; Cioslowski, J.; Ortiz, J. V.; Stefanov, B. B.; Liu, G.; Liashenko, A.; Piskorz, P.; Komaromi, I.; Gomperts, R.; Martin, R. L.; Fox, D. J.; Keith, T.; Al-Laham, M. A.; Peng, C. Y.; Nanayakkara, A.; Gonzalez, C.; Challacombe, M.; Gill, P. M. W.; Johnson, B. G.; Chen, W.; Wong, M. W.; Andres, J. L.; Head-Gordon, M.; Replogle, E. S.; Pople, J. A. *Gaussian 98*, revision A.7; Gaussian, Inc.: Pittsburgh, PA, 1998.
(26) (a) Becke, A. D. *J. Chem. Phys.* **1993**, *98*, 5648−5652. (b) Perdew, J. P.; Wang, Y. *Phys. Rev. B* **1992**, *45*, 13244.
(27) Hariharan, P. C.; Pople, J. A. *Theor. Chim. Acta* **1973**, *28*, 213.
(28) (a) Dewar, M. J. S.; Thiel, W. *J. Am. Chem. Soc.* **1977**, *99*, 4907−4917. (b) Davis, L. P.; Guidry, R. M.; Williams, J. R.; Dewar, M. J. S.; Rzepa, H. S. *J. Comp. Chem.* **1981**, *2*, 433−445.

Table 2. Optimized Values of the Most Important Bond Lengths of Adsorbed Olefins (angstroms), Calculated Vibrational Frequencies (cm^{-1}),[a] and Adsorption Energies (E_{ads} in kcal/mol)[b,c]

	T1A	T1B	T2A	T2B	T2C	T4A	T4B
				ethene			
$r(O_aH)$	0.992	0.992	0.997	0.992	0.996	0.993	0.997
$r(HC_a)$	2.186	2.227	2.160	2.244	2.158	2.158	2.105
$r(HC_b)$	2.211	2.232	2.213	2.356	2.174	2.215	2.116
$r(C_aC_b)$	1.337	1.337	1.337	1.336	1.337	1.337	1.338
$a(AlO_aSi)$	134.2	140.0	142.0	141.2	129.1	135.0	136.2
ν(OH)	3208.7	3226.1	3123.3	3239.7	3168.6	3191.2	3101.4
ν(CC)	1619.4	1620.8	1617.8	1622.8	1619.4	1620.1	1617.4
E_{ads}	−3.54	−3.52	−4.22	−1.08	−3.97	−4.18	−5.77
				propene			
$r(O_aH)$	0.992	0.994	0.996	0.993	0.999	0.998	1.003
$r(HC_a)$	2.176	2.142	2.193	2.153	2.040	2.116	2.006
$r(HC_b)$	2.342	2.359	2.406	2.592	2.230	2.268	2.183
$r(C_aC_b)$	1.340	1.341	1.340	1.340	1.342	1.342	1.343
$a(AlO_aSi)$	133.4	139.6	141.7	140.6	129.0	134.4	136.0
ν(OH)	3212.7	3183.4	3092.7	3205.7	3061.2	3100.4	3000.2
ν(CC)	1637.6	1636.3	1636.4	1639.9	1633.2	1634.9	1630.9
E_{ads}	−2.20	−2.87	−3.27	−0.08	−4.16	−4.24	−6.43
				isobutylene			
$r(O_aH)$	0.990	0.994	1.000	1.003	1.004	0.999	1.007
$r(HC_a)$	2.161	2.083	2.088	1.999	1.935	2.073	1.939
$r(HC_b)$	2.803	2.710	2.679	2.620	2.431	2.506	2.332
$r(C_aC_b)$	1.344	1.345	1.345	1.346	1.347	1.347	1.348
$a(AlO_aSi)$	133.1	139.1	141.1	140.5	128.9	134.1	135.0
ν(OH)	3250.0	3173.5	3055.2	3007.1	2957.4	3085.9	2912.6
ν(CC)	1641.7	1640.1	1634.7	1633.5	1632.8	1632.0	1627.9
E_{ads}	1.89	−0.24	0.24	1.01	−0.36	−1.54	−5.6

[a] Scaled by 0.9573.[32] The calculated ν(CC) values for the free olefines are 1644.9, 1665.6, and 1672.2 cm^{-1} for ethene, propene, and isobutylene, respectively. [b] The atom labeling is shown in Chart 1. [c] The optimized C_aC_b bond lengths for isolated ethene, propene, and isobutylene are 1.329, 1.332, and 1.336 Å, respectively.

model are directly comparable and indicative of the stability of the site. It can be seen that the difference in DPE between T4B and T4A of 7.3 kcal/mol at the MM level is reduced to 3.1 kcal/mol at the QM level. On the contrary, T2B and T2C become 4.3 and 5.4 kcal/mol, respectively, more stable than T2A at the QM level. From these QM calculations it could appear that, from a thermodynamic point of view, the most abundant Brønsted acid sites would be those associated with positions T1A, T1B, T2B, and T2C. However, the small differences in energy found and the fact that the maximum for the ν(OH) band is found experimentally in the 3600−3612 cm^{-1} range[29] have caused us to consider in our study all the accessible acid sites in mordenite.

3.2. Olefin Adsorption. The interaction of the olefin double bond with the zeolite Brønsted acid site results in formation of a complex of π nature (structure I in Chart 1). It can be seen in Table 2 that the optimized geometries of the olefins and the bridging hydroxyl groups in the π complexes are very similar to those calculated for the isolated systems. The most important changes observed by formation of the complexes are the lengthening of both the C_aC_b and the O_aH bond lengths, which result in a decrease in the calculated ν(CC) and ν(OH) vibrational frequencies. In all cases, the proton of the bridging hydroxyl is closer to the primary carbon that is going to be protonated (C_a) than to the carbon atom that will interact with the basic oxygen (C_b). The H--C_a distances do not vary with increasing olefin size, but the H--C_b distances increase considerably due to steric repulsions between the methyl groups and the catalyst wall.

Adsorption of ethene and propene on the different mordenite acid sites considered is exothermic by 2−4 kcal/mol in most cases. However, adsorption of the bulkier isobutylene becomes more difficult and is energetically disfavored in some cases. It can be seen in Figure 2 that there is a good linear relationship between adsorption energies and H- -olefin double bond distance, calculated as $0.5(r(\text{H--C}_a) + r(\text{H--C}_b))$. The results shown in Table 2 suggest that there are two special positions in mordenite in which olefin adsorption is either specially difficult (T2B) or favored (T4B). The H atom of the T2B acid site is located on O22 (see Figure 1b), pointing to the center of the 8-T ring. There is probably a repulsion between the electron density of the two O24 oxygen atoms in this region, which are separated by only 4.809 Å, and the electrons in the π double bond of the adsorbed olefin. On the contrary, the H atom of the T4B site is located on O44, directly pointing to the center of the 12-T main channel, and allowing the formation of a strong complex with the three olefins.

The decrease in ν(CC) and ν(OH) vibrational frequencies accompanying formation of the π-complex is proportional to the strength of the interaction between the probe molecule and the acid site and has been considered as a measurement of the acidity of the site.[30,31] Figure 2 shows the fair relationships between calculated adsorption energies and $\Delta\nu$(OH) and $\Delta\nu$(CC) shifts obtained for ethene, propene, and isobutylene adsorption in mordenite.

3.3. Covalent Alkoxides. As shown in Chart 1, protonation

(29) Zholobenko, V. L.; Makarova, M. A.; Dwyer, J. *J. Phys. Chem.* **1993**, *97*, 5962−5964.
(30) Wakabayashi, F.; Kondo, J.; Wada, A.; Domen, K.; Hirose, C. *J. Phys. Chem.* **1993**, *97*, 10761−10768.
(31) Zecchina, A.; Geobaldo, F.; Spoto, G.; Bordiga, S.; Ricchiardi, G.; Buzzoni, R.; Petrini, G. *J. Phys. Chem.* **1996**, *100*, 16584−16599.
(32) Scott, A. P.; Radom, L. *J. Phys. Chem.* **1996**, *100*, 16502−16513.

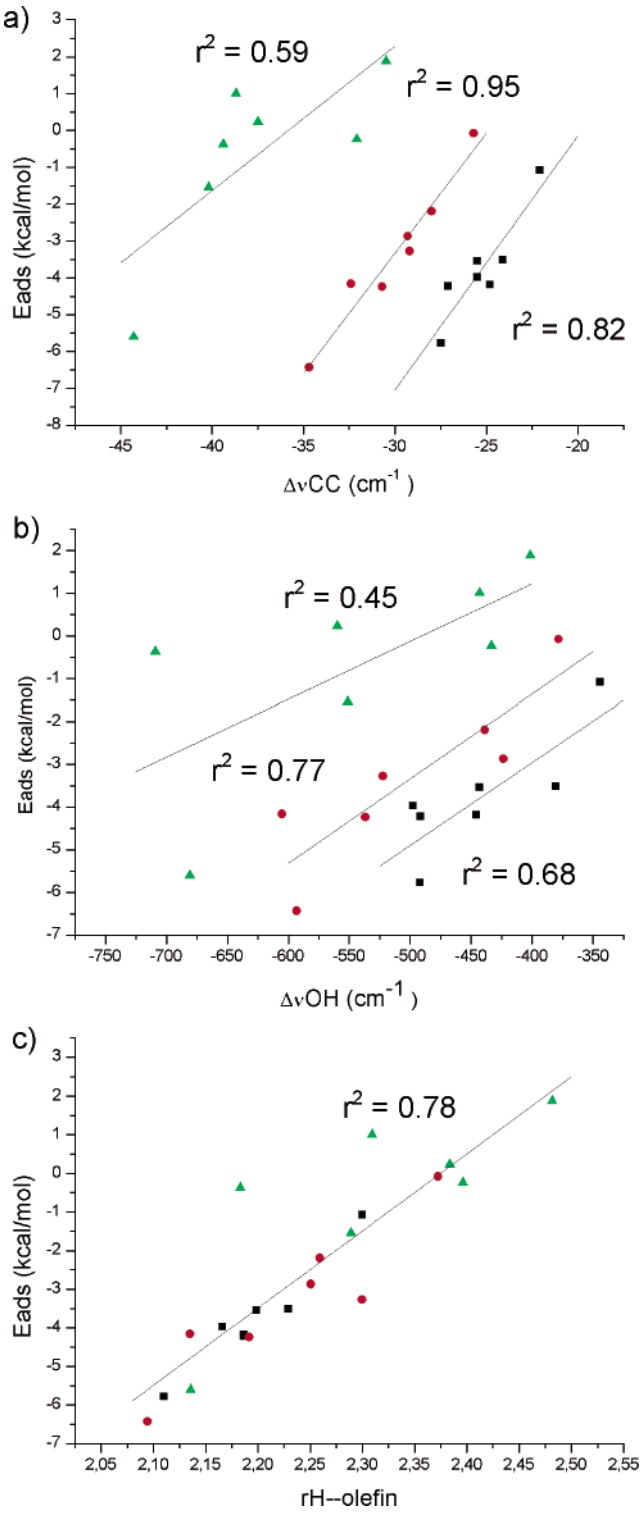

Figure 2. Plots of olefin adsorption energies (E_{ads} in kcal/mol)) versus (a) variation in the CC stretching frequency ($\Delta\nu$(CC) in cm^{-1}), (b) variation in the OH stretching frequency ($\Delta\nu$(OH) in cm^{-1}), and (c) H- -olefin double bond distance (in angstroms). Squares correspond to ethene, circles to propene, and triangles to isobutylene. The correlation coefficients r^2 for the linear relationships obtained are also shown.

of an adsorbed olefin I by the Brønsted acid site (O_a−H) may result in formation of an alkoxide complex III in which the positively charged C_b atom is covalently bound to another framework O atom (O_b). Table 3 summarizes the optimized geometries and the relative energies of the alkoxide complexes formed on the seven mordenite sites considered in this work, and Table 1 shows the labeling of the O_b atom in each site.

There is a strong influence of both the size and nature of the initial olefin and the position of the active site on the optimized geometries and stabilities of the alkoxide complexes formed. With respect to the organic molecule considered, it can be observed that the C_bO_b distances increase from ∼1.51 Å in ethene to ∼1.55 in propoxide and ∼1.62 Å in *tert*-butoxide. Also, the AlO_bSi angle closes between 5 and 12°, and the C_bO_bAl angle opens, especially in the case of *tert*-butoxide. The changes in the relative energies of the alkoxide complexes with respect to the adsorbed olefins (E_{alc}) are still more important. Thus, while ethoxide is in most cases more stable than adsorbed ethene, the E_{alc} values for propoxide range between −6.5 and 15.7 kcal/mol, and *tert*-butoxide is always considerably less stable than adsorbed isobutylene. This destabilization of the bulkier alkoxides can be related to the steric repulsions existing between the methyl groups and the zeolite wall, which cause an increase in the C_bO_b distances and therefore a weakening of the covalent CO bond. In agreement with this suggestion, it can be seen in Table 3 that the positive charge on the organic fragment in *tert*-butoxide is always higher than that in propoxide and in ethoxide, indicating a slightly more ionic character of the bulkier complexes.

The position of the O_b atom in the mordenite framework has also a strong influence on the stability of alkoxide complexes. It can be seen in Table 3 that the most stable ethoxide and propoxide complexes are those in which the C_b atom is attached to O24 in T2A and T2B sites. T1 and T4 positions are also favorable for formation of ethoxide, but not for propoxide or *tert*-butoxide. Finally, protonation of an olefin adsorbed on T2C always leads to an unstable alkoxide, no matter whether it is bonded to O12 or to O22. It was even impossible to obtain optimized structures for *tert*-butoxide complexes on these positions.

To know which parameters determine the stability of the alkoxide complexes on different sites, plots of calculated E_{alc} versus C_bO_b distances, AlO_bSi angles, and AlO_bSi angles in the deprotonated zeolite are shown in Figure 3. It can be seen that, as previously suggested, the stability of a given alkoxide decreases with increasing C_bO_b distance. Fair linear relationships between E_{alc} and rC_bO_b have been obtained for ethoxide and propoxide. In the case of *tert*-butoxide the correlation is worse, indicating that other factors have an important impact in this system.

As shown in Figure 3, fair linear relationships have also been obtained between E_{alc} and the AlO_bSi angle in the complex, and still better relationships have been obtained between E_{alc} and the AlO_bSi angle in the deprotonated zeolite. It seems that the most stable akoxides are those in which the AlO_bSi angle is about 126°, although the alkoxide formation in mordenite is favorable for angles up to approximately 132°. The most interesting result is that the capacity to achieve such small angles is already marked by the structure and geometry of the deprotonated zeolite. Thus, the Al−O24−Si angle, on which the most stable alkoxides are formed, is as small as 130.1° in the deprotonated zeolite, so that the deformation produced during alkoxide formation is not too important. On the other hand, AlO_bSi angles larger than 150° in the deprotonated zeolite are not able to become smaller than ∼132° during formation of

Table 3. Optimized Values of the Most Important Geometric Parameters of Covalent Alkoxides (distances in angstroms and angles in degrees), Calculated Relative Energies (E_{alc} in kcal/mol) with Respect to Adsorbed Olefins, and Mulliken Charges (|e|)[c]

	T1A	T1B	T2A	T2B	T2C	T4A	T4B
				ethoxide			
$r(O_bC_b)$	1.510	1.501	1.503	1.503	1.518[a] 1.527[b]	1.503	1.503
$a(C_bO_bAl)$	110.4	108.9	110.6	110.7	109.5[a] 106.4[b]	111.0	111.2
$a(AlO_bSi)$	131.5	128.9	126.0	125.9	134.5[a] 136.0[b]	131.4	130.1
E_{alc}	−2.11	−4.88	−13.72	−12.48	2.92[a] 1.68[b]	−7.49	−7.75
*q*org	0.316	0.320	0.325	0.325	0.321[a] 0.321[b]	0.330	0.323
				propoxide			
$r(O_bC_b)$	1.561	1.553	1.544	1.544	1.572[a] 1.579[b]	1.536	1.546
$a(C_bO_bAl)$	111.7	110.2	103.8	103.8	104.1[a] 111.8[b]	120.3	111.2
$a(AlO_bSi)$	127.9	124.6	125.4	125.4	133.7[a] 130.5[b]	127.7	126.5
E_{alc}	5.00	7.45	−6.47	−5.23	15.69[a] 11.51[b]	−2.65	1.38
*q*org	0.343	0.337	0.338	0.338	0.348[a] 0.351[b]	0.336	0.341
				tert-butoxide			
$r(O_bC_b)$	1.657	1.617	1.615	1.615		1.608	1.616
$a(C_bO_bAl)$	118.7	119.4	114.6	114.6		115.1	116.5
$a(AlO_bSi)$	121.4	117.3	120.6	120.6		123.5	124.1
E_{alc}	22.96	39.05	9.03	12.63		7.06	15.47
*q*org	0.387	0.360	0.373	0.373		0.378	0.374
				deprotonated zeolite			
$aAlO_bSi$	150.2	138.5	130.1	130.1	154.9[a] 154.1[b]	140.9	138.9

[a] C_b = O12. [b] C_b = O22. [c] The atom labeling is shown in Chart 1.

the alkoxide. Consequently, the stability of this alkoxide, if formed, will be much lower as it is indeed found in the calculations. This result is of practical interest because it allows us to predict, knowing the geometry of a deprotonated zeolite structure, in which positions it will be possible to obtain stable alkoxide complexes and in which positions it will not.

The plots in Figure 3 suggest that there are other factors influencing the stability of *tert*-butoxide complexes. For example, the most stable *tert*-butoxide is not formed on O24 as it occurs with ethoxide or propoxide, but on O44 (see Figure 1), by protonation of isobutylene adsorbed on T4A. The reason for this is that any organic fragment attached to O44 points directly to the center of the 12-T main channel, minimizing the steric repulsions with other framework atoms. These repulsions are not usually important in the case of ethoxide, but can explain the difference in stability of propoxide on T4A and T4B and most of the results obtained for *tert*-butoxide. Something similar occurs when the Al atom is located in T1. The large Al−O12−Si of T1A in the deprotonated zeolite (150.2°) suggests that alkoxides will be more easily formed on O11 (T1B site). This is true for ethoxide, but not for propoxide or for *tert*-butoxide, the difference of energy between the two complexes in this last case being as high as 16 kcal/mol. Figure 1 shows the situation of O11 in the narrow part of the elliptic 12-T ring. The two O12 oxygen atoms in this region are separated by only 5.225 Å, and there will probably be a destabilizing interaction between their electron density and that of the alkoxide complex formed. In the case of *tert*-butoxide, this repulsion is so important that the AlO_bSi angle closes to 117.3°, with a considerable energy cost.

3.4. Transition States for Olefin Protonation. As shown in Chart 1, adsorbed olefins I are converted into covalent alkoxides III through ionic transition states such as II, following a concerted mechanism. In one step, the hydrogen atom of the bridging hydroxyl group protonates the primary carbon atom of the olefin double bond (C_a), and simultaneously, the positive charge that appears on C_b interacts with one of the neighboring basic oxygen atoms of the zeolite (O_b), resulting in formation of a covalent alkoxide complex. The optimized geometries, atomic charges, and activation energies calculated for the transition states for protonation of ethene, propene, and isobutylene by acidic mordenite are summarized in Table 4, and Figure 4 shows the relationships between activation energies and atomic charges or selected geometric parameters. Despite all our efforts, it was impossible to localize the transition state for protonation of isobutylene adsorbed on T1B.

All the results indicate that calculated activation energies are directly related to the ionic character of the transition state and to the ability of the C_b carbon atom to stabilize the positive charge. Thus, activation energies follow the order ethene > propene > isobutylene, reflecting the order of stability of primary, secondary, and tertiary carbenium ions. For a given molecule, longer O_aH and shorter HC_a distances coincide with lower *q*H values and indicate that the proton-transfer process is more advanced. Also, C_aC_b bond lengths are longer and qC^+ values are higher, reflecting the rupture of the olefin double bond and the formation of the carbenium ion. The linear relationships between E_{act} and *q*H, qC^+, rO_aH, and rC_aC_b depicted in Figure 4 show that the more advanced the proton-transfer process, the larger the activation energy.

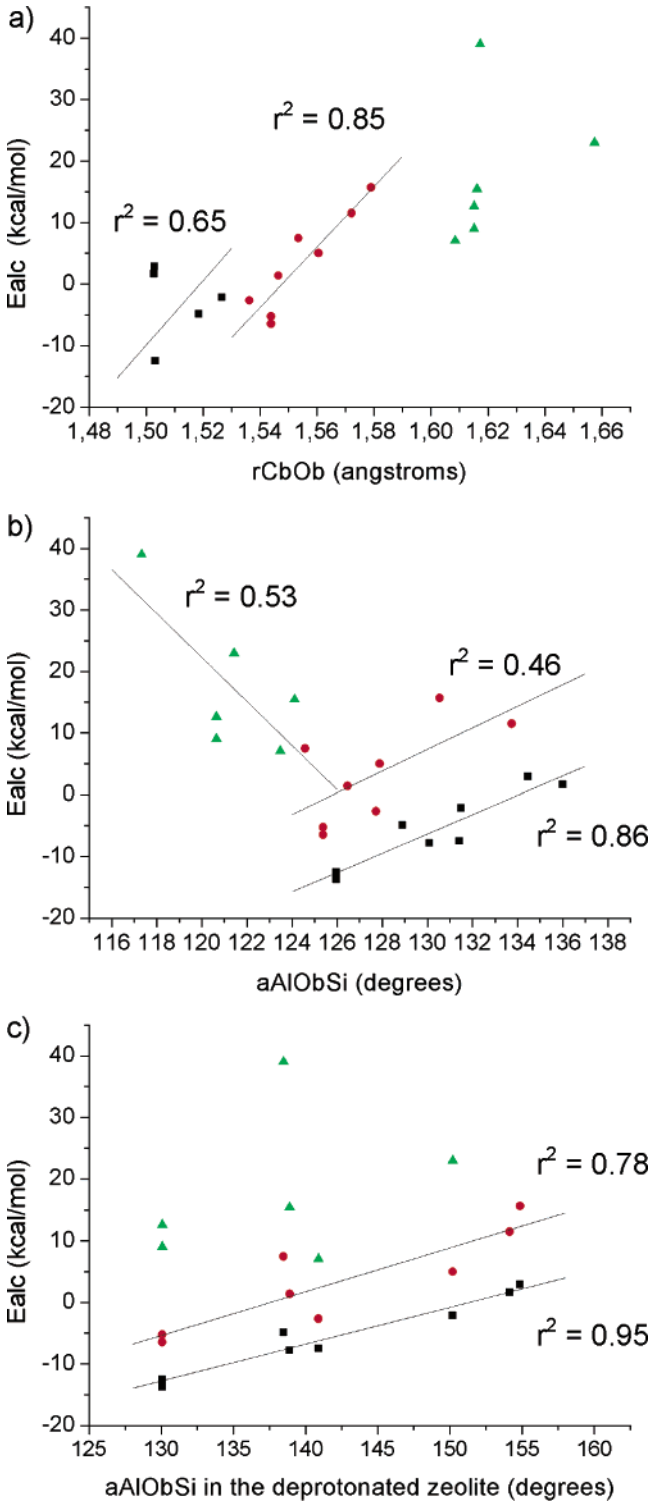

Figure 3. Plots of alkoxide−olefin energy difference (E_{alc} in kcal/mol)) versus (a) C_bO_b distance (in angstroms), (b) AlO_bSi angle in the alkoxide (in degrees), and (c) AlO_bSi angle in the deprotonated zeolite (in degrees). Squares correspond to ethoxide, circles to propoxide, and triangles to *tert*-butoxide. The correlation coefficients r^2 for the linear relationships obtained are also shown.

For ethene and propene, there is also a fair correlation between activation energy and rC_bO_b, a parameter that reflects the degree of formation of the alkoxide covalent bond. Optimized rC_bO_b distances in structure II are longer for propene than for ethene protonation. At the same time, the degree of proton transfer is higher in the case of propene protonation, and as a consequence the total positive charge on the C3 fragment is between 0.1 e and 0.2 e larger than that on the C2 system. However, the oposite trend is found for isobutylene protonation. The rO_aH and rHC_a distances are the shortest and the longest, respectively, reflecting a small degree of proton transfer, the total atomic charges on the organic fragments are similar to those obtained for the C2 transition states, and the CO distances are in all cases longer than 3 Å.

A deeper analysis of the imaginary vibrational modes that characterize all these structures as transition states also shows differences between isobutylene and the smaller olefins protonation. In the case of ethene and propene protonation, the only imaginary mode is associated with both the movement of the hydrogen atom that is being transferred from the zeolite to the olefin and the movement of the C_b atom toward the O_b atom to form the covalent alkoxide bond. But in the case of isobutylene protonation, the imaginary mode is only associated with the movement of the hydrogen atom from the zeolite to the olefin, indicating that the reaction product is not the *tert*-butoxide complex, but a free *tert*-butyl carbenium ion. In the following section, the complete mechanism for isobutylene protonation by acidic mordenite is studied in detail.

3.5. Carbenium Ion Intermediates. The imaginary vibrational modes associated with the reaction coordinate in the transition states for isobutylene protonation in mordenite indicate that the reaction products are not covalent alkoxides, but free *tert*-butyl carbenium ions (structure IV in Chart 1). The optimized values of the most important geometric parameters of these carbenium ions are summarized in Table 5 together with calculated net atomic charges. The energy profiles for olefin protonation are depicted in Figure 5 and the energies involved are given in Table 6.

The optimized geometries of the carbenium ions inside mordenite are very similar to that of the isolated *tert*-butyl cation. The three CC_bC angles in each of the adsorbed structures are in all cases between 119 and 121°, and the C_bCCC dihedral angles are close to zero, indicating a planar conformation of the molecule. The C_b atom, on which the positive charge is located, is situated more or less equidistant from all the accessible O atoms bonded to Al (two O atoms in the case of T1 and three O atoms for T2 or T4). The calculated C_b--O distances are always large, between 3.0 and 3.8 Å, suggesting that there are no strong interactions between the positively charged C_b atom and the framework oxygens. It is more likely that the negative charges on the oxygen atoms bonded to Al interact with the hydrogen atoms of the methyl groups. Table 5 shows all the calculated O--H distances shorter than 3 Å. In all structures there is at least one strong hydrogen bond with a O--H distance shorter than 2 Å and a stretched C−H bond, and one or two other weaker interactions of this type. The CC_b bond lengths in the adsorbed carbenium ions are also related to these hydrogen interactions. The longer the C−H bond in the methyl group, the shorter the CC_b distance.

It seems that there is not a completely clear relationship between the stability of the *tert*-butyl carbenium ions in mordenite and the number and strength of the hydrogen interactions with the oxygen atoms bonded to Al. The shortest O--H and longest C−H distances are found in the carbenium ions adsorbed on T1, which are the less stable with respect to the corresponding adsorbed isobutylene. On the other side, the

Table 4. Optimized Values of the Most Important Geometric Parameters (distances in angstroms and angles in degrees), Mulliken Charges (|e|), and Calculated Activation Energies (E_{act} in kcal/mol) of the Transition States for the Olefin Protonation Reaction[a]

	T1A	T1B	T2A	T2B	T2C[b]	T4A	T4B
				C_2			
$r(O_aH)$	1.481	1.501	1.368	1.419	1.351	1.396	1.420
$r(HC_a)$	1.204	1.197	1.296	1.270	1.196	1.259	1.242
$r(C_aC_b)$	1.403	1.403	1.385	1.385	1.407	1.394	1.395
$r(C_bO_b)$	2.214	2.191	2.358	2.359	2.198	2.235	2.251
$a(AlO_aSi)$	137.8	145.6	128.2	144.4	133.5	135.8	137.7
$a(AlO_bSi)$	135.6	129.9	131.1	129.6	134.5	135.7	132.8
qH	0.320	0.304	0.349	0.339	0.292	0.345	0.341
qC^+	0.315	0.328	0.237	0.247	0.341	0.281	0.285
$q$org	0.698	0.700	0.641	0.668	0.737	0.658	0.678
E_{act}	21.85	22.17	12.86	14.40	23.05	17.91	16.84
				C_3			
$r(O_aH)$	1.718	1.741	1.490	1.401		1.601	1.681
$r(HC_a)$	1.145	1.142	1.249	1.296		1.188	1.155
$r(C_aC_b)$	1.426	1.427	1.391	1.382		1.412	1.425
$r(C_bO_b)$	2.477	2.401	2.789	2.734		2.574	2.447
$a(AlO_aSi)$	137.8	146.1	144.3	142.8		136.0	139.6
$a(AlO_bSi)$	135.8	130.1	131.0	131.1		136.7	131.5
qH	0.270	0.261	0.335	0.350		0.310	0.286
qC^+	0.344	0.353	0.171	0.157		0.301	0.333
$q$org	0.867	0.864	0.746	0.669		0.842	0.860
E_{act}	18.97	18.72	9.44	8.38		12.70	15.02
				i-C_4			
$r(O_aH)$	1.426		1.316	1.357	1.452	1.413	1.462
$r(HC_a)$	1.264		1.346	1.321	1.246	1.271	1.251
$r(C_aC_b)$	1.396		1.388	1.384	1.396	1.397	1.400
$r(C_bO_b)$	3.275						
$a(AlO_aSi)$	133.3		141.6	141.5	129.6	134.6	135.8
$a(AlO_bSi)$	142.1						
qH	0.361		0.356	0.353	0.343	0.348	0.323
qC^+	0.144		0.063	0.038	0.107	0.156	0.157
$q$org	0.701		0.589	0.618	0.719	0.703	0.738
E_{act}	10.75		3.09	4.64	5.79	6.58	8.23

[a] The atom labeling is shown in Chart 1. [b] C_b = O12.

tert-butyl cation adsorbed on T4B, in which there are three quite strong hydrogen interactions, is slightly less stable than that adsorbed on T4A, in which there are only two such interactions of similar strength. However, a very direct relationship between the relative energy of the carbenium ions with respect to the adsorbed olefins and the total charge on the organic fragments has been found, indicating that carbenium ions inside mordenite are mainly stabilized by short- and medium-range electrostatic effects.

With respect to the nature of the adsorbed *tert*-butyl cations, they have been characterized as minima on the potential energy surface by means of frequency calculations and can therefore be considered reaction intermediates. Small imaginary modes with frequencies lower than 100 cm^{-1} have been obtained in some cases but, as previously explained, they are related to the movement of the framework atoms whose position is not optimized in the calculations, and not to the atoms involved in the mechanism.

All these data show that the concerted mechanism according to which an adsorbed olefin I is directly converted through transition state II into a covalent alkoxide III is valid for ethene and propene protonation by acidic mordenite. But the complete mechanism for isobutylene protonation is more complicated and involves a carbenium ion IV as reaction intermediate. The energy profiles for the two mechanisms are depicted in Figure 5. It can be seen that the *tert*-butyl carbenium ion intermediate should be converted into the *tert*-butoxide complex through a different transition state II′. It has been possible to localize this second transition state in the case of T2 (A and B), T4A, and T4B positions, but not in the case of T1. The optimized geometries of the transition states obtained are very similar to those of the adsorbed carbenium ions, the main difference being the shorter C_b-O_b distance (2.096, 2.243, and 2.203 Å in T2 (A and B), T4A, and T4B, respectively). The three CC bond lengths in each structure are equivalent and about 1.48 Å, the CCC angles are between 116 and 121°, and the CCCC dihedral angle is between 15 and 20°, reflecting a small distortion from planarity.

Table 6 summarizes the energies involved in the isobutylene protonation reaction profile depicted in Figure 5. The first remarkable result is that transition state II is in most cases slightly more stable than reaction intermediate IV. To check whether this surprising result is a consequence of the different way in which the ONIOM scheme treates the atoms belonging to different layers, single point calculations at the B3PW91/6-31G(d,p) level have been performed on all the structures involved in the mechanism. The activation energies calculated at this theoretical level (full DFT in Table 6) are quite similar to those obtained using the ONIOM method, but the relative energies for the *tert*-butyl carbenium ions decrease, and therefore the reaction intermediate becomes in all cases more stable than the transition state for its formation. The larger stabilization of carbenium ions with respect to transition states could be attributed to a better treatment of short- and medium-range electrostatic effects in the full DFT calculations. Since the reaction intermediates are between 0.2 and 0.3 e more positively charged than the corresponding transition states, a greater influence of the electrostatic effects on their energy could be

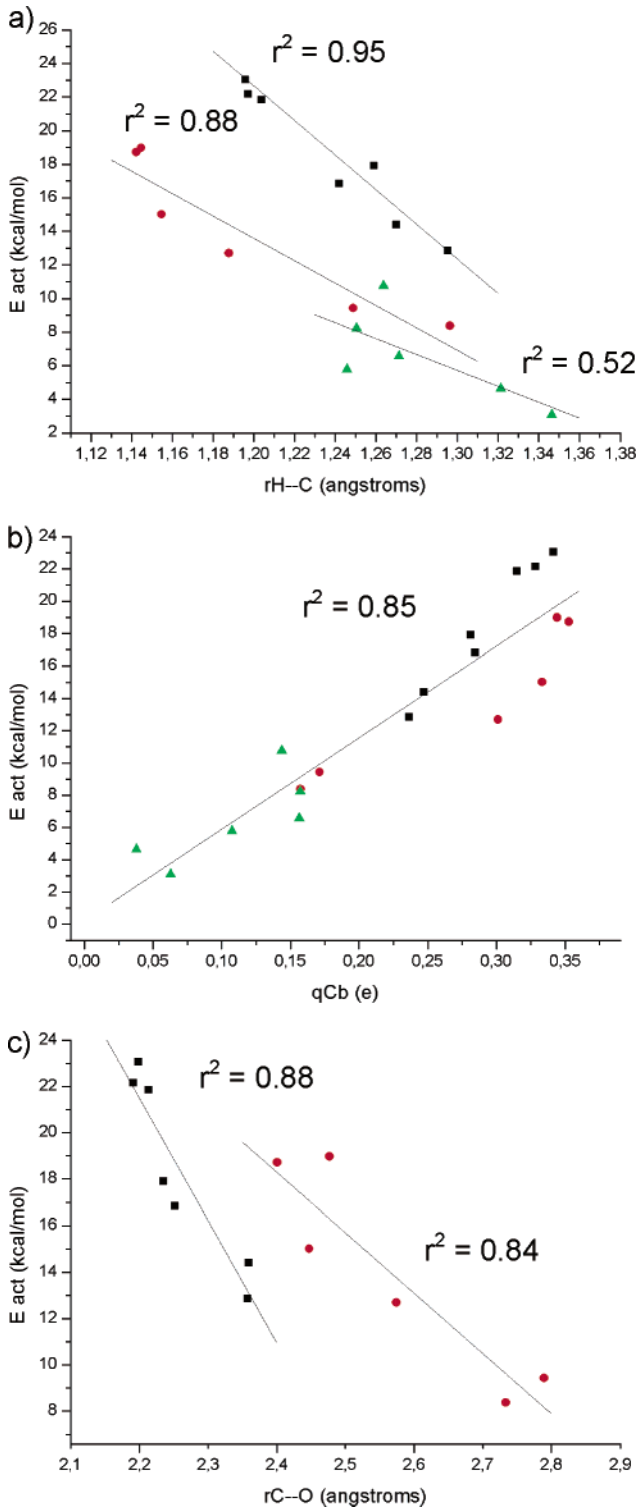

Figure 4. Plots of olefin protonation activation energies (E_{act} in kcal/mol)) versus (a) H--C_a distance (in angstroms), (b) net atomic charge on C_b (in |e|), and (c) C_bO_b distance (in angstroms). Squares correspond to ethene, circles to propene, and triangles to isobutylene. The correlation coefficients r^2 for the linear relationships obtained are also shown.

Table 5. Optimized Values of the Most Important Geometric Parameters (distances in angstroms and angles in degrees) and Mulliken Charges (|e|) of *tert*-Butyl Carbenium Ion Adsorbed on Different T Sites of Mordenite[a]

	T1A	T1B	T2A	T2B	T2C	T4A	T4B
$r(C_bO_a)$	3.592	3.489	3.679	3.538	3.403	3.508	3.224
$r(C_bO_b)$	3.238	3.405	3.403	3.487	3.679	2.978	3.503
$r(C_bO)$			3.567	3.783	3.567	3.760	3.816
$r(C_aC_b)$	1.427	1.408	1.444	1.432	1.446	1.443	1.444
$r(C_bC_m)$	1.465	1.470	1.446	1.453	1.444	1.455	1.457
$r(C_bC_m)$	1.470	1.473	1.470	1.475	1.470	1.469	1.459
$d(C_bC_aC_mC_m)$	−0.676	−6.137	1.635	2.692	1.635	−0.349	−6.570
$r(C_aH)$	1.153	1.192	1.137	1.143	1.124	1.137	1.115
$r(O_aH)$	1.752	1.664	1.927	1.886	1.926	1.837	2.114
$r(C_mH)$	1.108	1.103	1.124	1.125	1.137	1.127	1.139
		1.102					1.124
$r(O_bH)$	2.552	2.493	1.926	2.035	1.927	1.951[b]	1.859
		2.763					2.063
qC^+	0.264	0.220	0.273	0.251	0.273	0.300	0.280
$q$org	0.914	0.855	0.934	0.932	0.934	0.929	0.932

[a] The atom labeling is shown in Chart 1. [b] Not O_b.

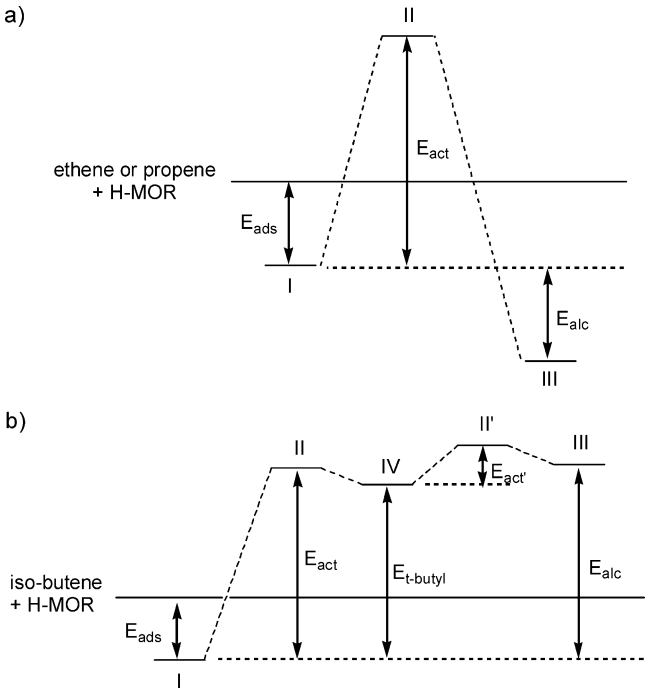

Figure 5. Energy profile for the protonation of (a) ethene, propene, and (b) isobutylene.

Table 6. Calculated Energies (kcal/mol) Corresponding to the Isobutylene Protonation Reaction Profile Depicted in Figure 5

	ONIOM				full DFT			
	E_{act}	$E_{t-butyl}$	$E_{act'}$	E_{alc}	E_{act}	$E_{t-butyl}$	$E_{act'}$	E_{alc}
T1A	10.75	11.48		22.96	7.76	6.36		16.88
T1B		17.18		39.05		9.11		25.51
T2A	3.09	0.87	9.15	9.03	5.54	1.79	7.02	8.94
T2B	4.64	6.40	6.68	12.63	5.20	2.42	6.39	9.00
T2C	5.79	6.88			5.62	5.50		
T4A	6.58	6.90	3.89	7.06	7.44	6.25	2.78	4.77
T4B	8.23	8.46	8.45	15.47	6.77	5.61	1.80	5.20

expected. However, it can be seen in Table 6 that, in some cases, the covalent alkoxides are also considerably stabilized by the full DFT calculations.

The largest differences between the ONIOM and the full DFT results are found for the *tert*-butyl cation and *tert*-butoxide complex located on T1B, whose optimized structures are depicted in Figure 6. In both cases, there are several H atoms of the methyl groups orientated toward framework oxygens not linked to the Al atom and with calculated O--H distances between 2.5 and 3.0 Å. These O atoms belong to the low-level layer in the ONIOM scheme and are therefore calculated at the semiempirical MNDO method, which might not correctly

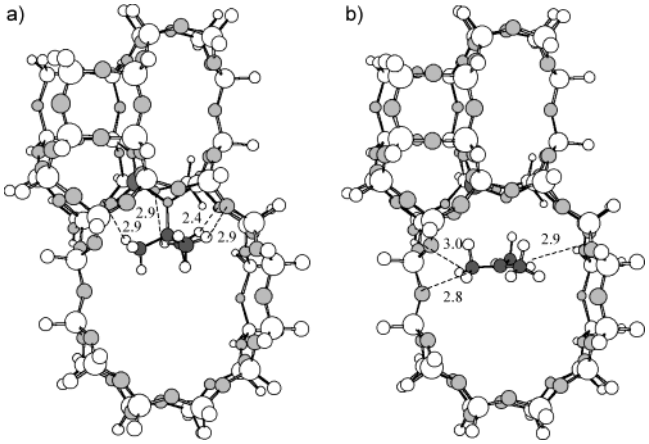

Figure 6. Optimized structure of *tert*-butoxide covalent complex (a) and *tert*-butyl carbenium ion (b) on the T1B site. Only distances between atoms belonging to different layers in the ONIOM scheme are shown.

describe hydrogen bonding. Within this approach, these O--H interactions are not well treated, and the stability of the whole system is underestimated. Something similar happens with the carbenium ion adsorbed on T1A and with the alkoxide complexes located on T1A and T4B. On T1A, there are short distances between the hydrogen atoms of the methyl groups and the O24 and O44 framework oxygens (see Figure 1), while on T4B the framework oxygen involved is O22. In the other T positions there are no such interactions, and therefore, the energy differences between the ONIOM and full DFT results are not so important.

Considering the full DFT results, it was found that the energy profile for isobutylene protonation by mordenite and the product obtained in the reaction varies depending on the T position on which the Al atom is located. If the Al atom occupies the T1 position, isobutylene is protonated with an activation energy of 7.76 kcal/mol to give an adsobed carbenium ion 6.36 kcal/mol less stable than the initial reactant, while formation of covalent *tert*-butoxide complexes is completely disfavored. When the Al atom is located on T2, protonation of isobutylene occurs with an activation energy of ∼5 kcal/mol, and adsorbed *tert*-butyl carbenium ions only ∼2 kcal/mol less stable than the initial reactants are obtained as reaction products. The transformation of these carbenium ions in covalent alkoxides is possible but difficult, due to the high activation energies and the fact that the reaction is endothermic by about 9 kcal/mol. However, if the Al atom is situated on T4, isobutylene is protonated to give a carbenium ion intermediate with an activation energy of ∼7 kcal/mol. In a second step, the carbenium ion is easily converted, with an activation energy of only 2−3 kcal/mol, into a slightly more stable covalent alkoxide, which will be the reaction product.

Finally, it is important to remark on the agreement between our results and those obtained by Rozanska et al.[20] using the periodic DFT approach. Their activation energy (E_{act}) and energy difference between *tert*-butyl cation and isobutylene adsorbed on the T4A site ($E_{t-butyl}$), 7.2 and 6.0 kcal/mol, respectively, are equivalent to our full DFT values.

4. Conclusions

The mechanism of protonation of ethene, propene, and isobutylene adsorbed on seven different Brønsted acid sites of mordenite has been studied using the ONIOM methodology to assess the influence of olefin size and local geometry of the active site on the species and energies involved.

The stability of the covalent alkoxides is marked by both the olefin size and the local geometry of the active site. As already known, alkoxide stability follows the order ethoxide > propoxide > *tert*-butoxide. With respect to the second factor, it has been found that the stability of a given alkoxide depends linearly on the AlO_bSi angle value in the complex, which in turn is determined by the corresponding value in the deprotonated zeolite. This means that it is possible to predict, from the geometry of the deprotonated zeolite, which positions in a zeolite will be favorable to formation of stable covalent intermediates. On the other side, activation energies are not so influenced by the local geometry of the active site, but are more directly related to the ionic character of the transition state and to the ability of the C_b carbon atom to stabilize the positive charge. Thus, they follow the order ethene > propene > isobutylene, reflecting the order of stability of primary, secondary, and tertiary carbenium ions.

It has also been shown that while protonation of ethene and propene follow the classical concerted mechanism according to which adsorbed olefins are converted into stable covalent alkoxide intermediates through carbenium ion-like transition states, protonation of isobutylene by a mordenite Brønsted acid site always results in formation of a free *tert*-butyl carbenium ion intermediate, which can be converted or not, depending on the location of the acid site in the zeolite, into the covalent *tert*-butoxide species through a different transition state. The nature of the carbenium ions has been characterized by means of frequency calculations, and in all cases they have been proven to be minima on the potential energy surface. However, the energy profile for isobutylene protonation by mordenite and the product obtained in the reaction (the *tert*-butyl carbenium ion or the *tert*-butoxide complex) will vary depending on the T position on which the Al atom is located. This new finding could explain for example why zeolites with the same structure and composition but synthesized with different methods show different catalytic behavior. The reason could be that the template and/or the conditions used in the synthesis of a zeolite may favor different positions for the Al atoms, and since the nature of the reaction intermediates depends on the position of the Al atoms, the catallytic activity or the products obtained with these zeolites might also be different.

From a methodological point of view, and by comparison of our ONIOM and full DFT results with periodic DFT calculations,[21] it can be concluded that the ONIOM scheme does not treat correctly the interactions between atoms belonging to different layers. However, single point calculations of the energy of the whole system at the same theoretical level yield results comparable to those of periodic calculations, provided the cluster used is large enough to include all short-range interactions between the molecule and the catalyst.

Acknowledgment. We thank the Departament de Química Física of the University of Valencia for computing facilities.

JA039432A